

Polynomial Representation for Persistence Diagram

Zhichao Wang^{1*}Qian Li^{2*}Gang Li³Guandong Xu²¹School of Electrical Engineering and Telecommunications, University of New South Wales, Australia²Advanced Analytics Institute, University of Technology Sydney, Australia³School of Information Technology, Deakin University, Geelong, VIC 3216, Australia

zhichao.wang2@unsw.edu.au {qian.li, guandong.xu}@uts.edu.au gang.li@deakin.edu.au

Abstract

Persistence diagram (PD) has been considered as a compact descriptor for topological data analysis (TDA). Unfortunately, PD cannot be directly used in machine learning methods since it is a multiset of points. Recent efforts have been devoted to transforming PDs into vectors to accommodate machine learning methods. However, they share one common shortcoming: the mapping of PDs to a feature representation depends on a pre-defined polynomial. To address this limitation, this paper proposes an algebraic representation for PDs, i.e., polynomial representation. In this work, we discover a set of general polynomials that vanish on vectorized PDs and extract the task-adapted feature representation from these polynomials. We also prove two attractive properties of the proposed polynomial representation, i.e., stability and linear separability. Experiments also show that our method compares favorably with state-of-the-art TDA methods.

1. Introduction

As a bridge between algebraic topology and statistical methods, topological data analysis (TDA) extracts the topological features that are complementary to statistical quantities [33, 36]. In the past several years, TDA has found many applications in areas including bioinformatics [6, 31, 38], computer vision [5, 14, 25, 28], audio signals [4, 29] and natural language processing [18, 40]. As one common approach to TDA, *persistent homology* captures the characteristics of data by the scales at which topological features (connected component, cycle, void, etc.) are born and the scales at which they die. A standard way to represent the persistent homology is through the *persistence diagram* (PD), which encodes the lifespan of every topological feature [13, 36]. However, PD cannot be straightforwardly

adopted in standard machine learning methods, because it is not in the vector space [1, 7].

Related work. To address this issue, considerable efforts have been devoted to mapping PDs into a vector space, and existing work can be categorized into three classes. Methods in the first class express PDs in the Hilbert space via kernel functions [7, 10, 26, 35]. For instance, a multi-scale heat kernel is defined for PDs through a L_2 -valued feature mapping, which thus can be used with the support vector machine (SVM) [35]. Alternately, a weighted Gaussian kernel is proposed to treat a PD as a discrete measure, and to control the effect of persistence in the PD [26]. The sliced Wasserstein kernel is also a Gaussian-type kernel defined by a modified Wasserstein distance between PDs [7]. Methods in the second class directly vectorize PDs in the Euclidean space [1, 2, 11, 15]. For instance, the persistence image [1] constructs \mathbb{R}^n representation by integrating a weighted density estimate of the PD into a persistence surface. Persistence square-root representation [2] models the PD as a 2D probability density function on the tangent vector space of Riemannian manifold. Deep neural networks is adopted to vectorizes PDs by defining input layer with stable property [24]. Methods in the third class represent PDs in the function space. For example, persistence landscapes (PLs) [11] are developed to construct the piecewise linear functions on PDs for further data analysis tasks. Another work [15] transforms PDs into complex polynomials of the function space.

Above vectorization methods consider the resulting vectors of PDs as the feature inputs for machine learning, and some of them achieve provable stability under the perturbations in PDs. However, most existing works focus on defining the polynomials with specific form (e.g. kernel map) for PDs, which may be suboptimum. Instead of *pre-defined* polynomials, how to extract more flexible or preferable polynomials from PDs for constructing discriminative features remains largely unexplored.

*Equal contribution

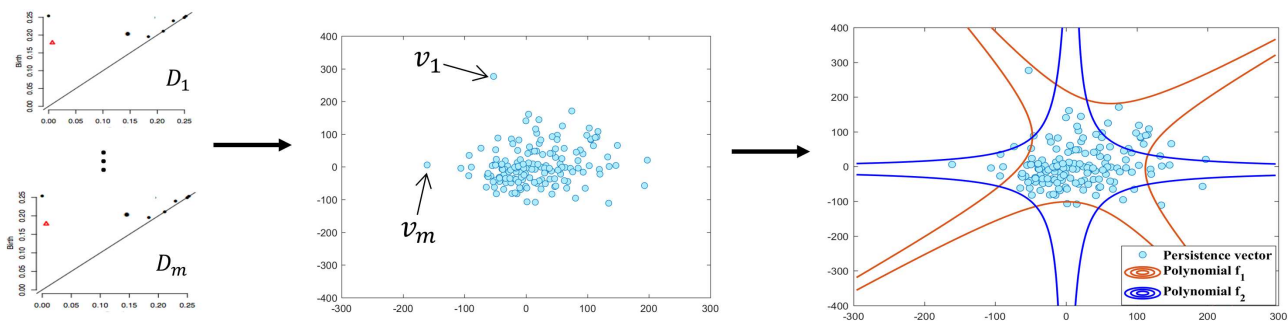


Figure 1. An example of polynomial representation for PDs. Assume m PDs $\{\mathcal{D}_i\}_{1 \leq i \leq m}$ belong to the same class, our method first derives m stable persistence vectors $\{v_i\}_{1 \leq i \leq m}$ from those PDs. Assume that two polynomials approximately vanish on those m persistence vectors, i.e., $f_1(v) \approx 0$ and $f_2(v) \approx 0$ for all v . Using those vanishing polynomials, our method can define the polynomial representation for PDs, which is proved to be linearly separable.

Contributions. To address these limitations, this paper proposes a task-oriented algebraic representation for PDs, namely *polynomial representation*, which extracts the stable and linearly separable features for PDs. As shown in Fig. 1, the proposed *polynomial representation* consists of two steps: *stable persistence vectorization* and *representation with vanishing polynomials*.

First, *stable persistence vectorization* transforms a PD into a persistence vector while maintaining interpretable connections. As a theoretical contribution, the persistence vector is proved to be stable with respect to perturbations in PDs. Second, the persistence vector is treated as the root of some general polynomials to construct the *polynomial representation* with the forms of nonlinear curves, surfaces and their unions. By exploiting the underlying nonlinear nature, *representation with vanishing polynomials* can extract the task-specific and discriminative features from the persistence vector. This also offers greater flexibility and representational power by deriving linearly separable feature, which can obviously improve the classification performance. In addition, an efficient algorithm is proposed to compute the *polynomial representation* from the persistence vectors. Numerical experiments on topological data analysis demonstrate the favorable performance of the proposed method.

2. Preliminary on Persistence Diagram

In this section, we give a brief overview of the persistence diagram, and leave more details in the supplementary. A comprehensive introduction can be found in [12, 13].

Topological data analysis (TDA) aims to infer complex topological features (connected components, cavities and higher-dimensional holes) directly from underlying data [16, 18]. Machine learning methods can also uncover the geometric structure of data, but they can only identify 0-dimensional topological structure, i.e., connected components. Unsupervised learning or clustering in machine

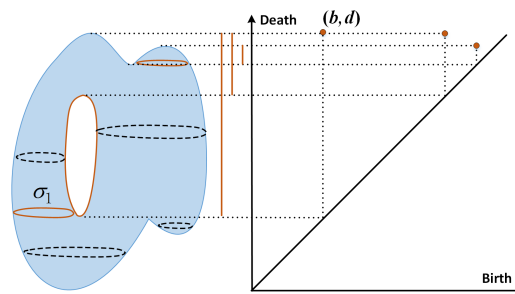


Figure 2. An example of persistence diagram.

learning can be viewed as the 0-dimensional holes of topological inference, i.e., the connectivity of the data. In general, for a more general topological space embedded in d -dimensional Euclidean space, there are d -different types of holes with dimension from 0 to $d-1$. For example, a sphere encloses a 2-dimensional hole while a circle encloses a 1-dimensional hole.

TDA can track how the topological features appear and disappear in a nested sequence of topological spaces. A standard descriptor to represent such topological evolution is **persistence diagram (PD)** [12, 13], which is in fact a multi-set of points in a plane. Each point (b, d) corresponds to the lifespan of one topological feature, where b and d are its birth time and death time, respectively. Points are entirely located in the half-plane above the diagonal, since the death time always occurs after the birth time.

Fig. 2 gives an example of PD with respect to a height function f on a surface. One way to understand the function f is through the topology of its sublevel sets $f^{-1}((-\infty, t])$. The sublevel set $f^{-1}((-\infty, t])$ can record such topological events, i.e., the cycle may create or merge when varying t from $-\infty$ to ∞ . We start with the 1-dimensional topological feature (i.e., cycle) carried by the sublevel sets. For instance, a point (b, d) is depicted in the PD corresponding to the 1-dimensional topological feature σ_1 . When t goes

through the height value b , the sublevel sets $f^{-1}((-\infty, b])$ that were homeomorphic to two discs become homeomorphic to the disjoint union of a disc and an annulus, creating a first cycle homologous to σ_1 . These two created cycles are never filled before t reaches the end of the filtration d . The interval between the birth time b and the death time d reflects the persistence (lifespan) of σ_1 . To understand the topological feature with more than one dimension, the preliminary of algebraic topology is required, please refer to [18, 22] for details. Points far from the diagonal represent the persistent topological features with long persistences, while points close to the diagonal can be considered as topological noise. The supplementary also provides an example of PD construction from point cloud data.

A popular metric to measure the similarity between two PDs is p -Wasserstein distance [34]. Points on the diagonal of PD are considered as a part of PD such that there exists bijections between two PDs [13, 35]. In general, this metric is expressed by minimizing the distance of any two corresponding points, over all bijections between two PDs.

Definition 1 [34] *Given two PDs \mathcal{D}_1 and \mathcal{D}_2 , let γ be a bijection between \mathcal{D}_1 and \mathcal{D}_2 . For any $p > 0$, the p -Wasserstein distance is*

$$d_{W,p}(\mathcal{D}_1, \mathcal{D}_2) = \inf_{\gamma: \mathcal{D}_1 \rightarrow \mathcal{D}_2} \left(\sum_{u \in \mathcal{D}_1} \|u - \gamma(u)\|_\infty^p \right)^{1/p} \quad (1)$$

Note that a bijection γ exists by matching points in \mathcal{D}_1 with points in \mathcal{D}_2 such that each point in \mathcal{D}_1 (resp. in \mathcal{D}_2) has to be matched, either to a unique point in \mathcal{D}_2 (resp. in \mathcal{D}_2), or to its nearest neighbor in the diagonal. One reason for the popularity of PDs in topological data analysis is that the transformation of a topological data into a PD is stable with respect to p -Wasserstein distance [13, 35].

PDs for machine learning. In fact, the space of PDs is a metric space with the p -Wasserstein distance [13, 35]. However, this metric space is neither a Euclidean space nor a Hilbert space [1, 7]. For machine learning methods such as SVM or PCA, the input data is supposed to be in the Euclidean space or Hilbert space. Therefore, PDs cannot be directly used as inputs for a variety of machine learning methods. To analyze topological features encoded in PDs, most statistical research works convert the PD into a vector [1, 7, 26, 36].

3. Stable persistence vectorization

The first part of the proposed *polynomial representation* is *stable persistence vectorization*. This novel vectorization method transforms the PD into a Euclidean vector while maintaining the interpretable connection with the original PD. The proposed vectorization is stable with respect to perturbations of PDs and also efficient to compute.

Recall that PD is a 2-dimensional plane with a set of points. A point (u_x, u_y) represents that a topological feature is born at time u_x and dies at u_y . All points (u_x, u_y) lie above the diagonal, since the birth must precede the death. Hence, $u_y - u_x$ defines the persistence of the topological feature. The point with a long persistence represents an important topological feature, while the point with a short persistence may represent the topological noise. To measure the importance of points in PDs, we propose a flexible weighting function as

$$\omega(u_x, u_y) = \arctan(C(u_y - u_x)^2) \quad (2)$$

where C is a non-negative parameter. The weighting function is non-decreasing with respect to the persistence of each PD point, which gives large weights for points with long-persistences to indicate its high significance in PDs. More importantly, \arctan is a bounded and continuous function, which is vital to guarantee the stability of the vectorization of PDs. Parameter C ensures that points with long persistences will have large weights, while points with short persistences will have small weights.

Based on the weight function, we construct a mapping from the PD to a finite-dimensional vector. To ensure that the resulting vector is stable w.r.t. permutations of PDs, the mapping needs to be Lipschitz continuous [13]. A standard strategy is to construct a kernel mapping via an exponential function [26, 35]. However, the kernel mapping is usually inefficient to compute. For computational efficiency, we use a simple exponential function to define a Lipschitz scalar function $\rho: \mathbb{R} \rightarrow \mathbb{R}$ as

$$\rho_{\mathcal{D}}(z) = \sum_{(u_x, u_y) \in \mathcal{D}} \omega(u_x, u_y) e^{-\frac{(u_x - z)^2}{\sigma^2}} \quad (3)$$

where σ is a width parameter. Eq. (3) defines the mean of exponential function u_x . Alternatively, one can use $u_y - z$ or $(u_x + u_y)/2 - z$ as the mean. All these choices do not change the stability of persistence vector with only a slight modification to the constants. With this scalar function, we define a novel persistence vector derived from a PD.

Definition 2 (Persistence vector) *Define the range $[a, b]$ that contains the ranges of the birth/death times of all points in the PDs. Let $I = b - a$, the n -dimensional persistence vector of a PD \mathcal{D} is defined as*

$$\mathbf{v}_{\mathcal{D}} := \frac{I}{n} \cdot [\rho_{\mathcal{D}}(a + \frac{I}{n}), \rho_{\mathcal{D}}(a + \frac{2I}{n}), \dots, \rho_{\mathcal{D}}(a + \frac{nI}{n})] \quad (4)$$

Note that the interval $[a, b]$ is defined to involve the ranges of birth/death times of points in all the PDs. For a specific PD \mathcal{D} , its persistence vector $\mathbf{v}_{\mathcal{D}}$ with dimension n is generated by computing the scalar function ρ over the discretized interval $[a, b]$. In that way, \mathbf{v} can evenly explore

the complete spatial information in PDs by uniformly being increased in the PD. More importantly, the ingredient I/n is crucial to ensure that persistence vector \mathbf{v} is stable with respect to small perturbations of PDs. In the following, the stability of persistence vector is given in Theorem 1.

Lemma 1 *Let $u = (u_x, u_y) \in \mathcal{D}_1$ be the point in PD, the point $v \in \mathcal{D}_2$ be the perturbed version of u . For ρ in Eq. (3), we have an exponential function $g_{u_x}(z) = e^{-\frac{(u_x - z)^2}{\sigma^2}}$ and a weighting function $\omega(u) = \arctan(C(u_y - u_x)^2)$. Let $K = \sqrt{2} \left(1 + \frac{\sqrt{\pi}}{\sigma}\right)$, then we have*

$$\int_{-\infty}^{\infty} |\omega(u)g_{u_x}(z) - \omega(v)g_{v_x}(z)| dz \leq K \|u - v\|_{\infty} \quad (5)$$

Proof See proof in the supplement.

With Lemma 1 in mind, we turn to prove the persistence vector is stable w.r.t. 1-Wasserstein distance between PDs.

Theorem 1 (Stability Theorem) *The persistence vector \mathbf{v} is stable w.r.t. the 1-Wasserstein distance $d_{W,1}$ between their PDs. In particular,*

$$\|\mathbf{v}_{\mathcal{D}_1} - \mathbf{v}_{\mathcal{D}_2}\|_1 \leq \sqrt{2} \left(1 + \frac{\sqrt{\pi}}{\sigma}\right) \cdot d_{W,1}(\mathcal{D}_1, \mathcal{D}_2)$$

$$\|\mathbf{v}_{\mathcal{D}_1} - \mathbf{v}_{\mathcal{D}_2}\|_2 \leq \sqrt{2} \left(1 + \frac{\sqrt{\pi}}{\sigma}\right) \cdot d_{W,1}(\mathcal{D}_1, \mathcal{D}_2)$$

$$\|\mathbf{v}_{\mathcal{D}_1} - \mathbf{v}_{\mathcal{D}_2}\|_{\infty} \leq \sqrt{2} \left(1 + \frac{\sqrt{\pi}}{\sigma}\right) \cdot d_{W,1}(\mathcal{D}_1, \mathcal{D}_2)$$

Proof 1-Wasserstein distance states that a bijection is required when comparing two PDs, i.e., \mathcal{D}_1 and \mathcal{D}_2 . Points on the diagonal are considered as a part of every persistence diagram \mathcal{D} such that there exists a bijection γ generating $\gamma(u) = (v_x, v_y) \in \mathcal{D}_2$ for $u = (u_x, u_y) \in \mathcal{D}_1$.

$$\begin{aligned} \|\mathbf{v}_{\mathcal{D}_1} - \mathbf{v}_{\mathcal{D}_2}\|_1 &= \frac{I}{n} \sum_{i=1}^n |\rho_{\mathcal{D}_1}(z_i) - \rho_{\mathcal{D}_2}(z_i)| \\ &\leq \int_{-\infty}^{\infty} |\rho_{\mathcal{D}_1}(z) - \rho_{\mathcal{D}_2}(z)| dz \\ &= \int_{-\infty}^{\infty} \left| \sum_{u \in \mathcal{D}_1} \omega(u)g_{u_x}(z) - \sum_{\gamma(u) \in \mathcal{D}_2} \omega(v)g_{v_x}(z) \right| dz \\ &\leq \sum_{u \in \mathcal{D}_1} \int_{-\infty}^{\infty} |\omega(u)g_{u_x}(z) - \omega(v)g_{v_x}(z)| dz \\ &\leq \sqrt{2} \left(1 + \frac{\sqrt{\pi}}{\sigma}\right) \cdot d_{W,1}(\mathcal{D}_1, \mathcal{D}_2) \quad (\text{By Lemma 1}) \end{aligned}$$

We now have the following relation

$$\|\mathbf{v}_{\mathcal{D}_1} - \mathbf{v}_{\mathcal{D}_2}\|_1 \leq \sqrt{2} \left(1 + \frac{\sqrt{\pi}}{\sigma}\right) d_{W,1}(\mathcal{D}_1, \mathcal{D}_2)$$

For vectors in \mathbb{R}^n , l_2 -norm and l_1 -norm follow

$$\|\mathbf{v}_{\mathcal{D}_1} - \mathbf{v}_{\mathcal{D}_2}\|_2 \leq \|\mathbf{v}_{\mathcal{D}_1} - \mathbf{v}_{\mathcal{D}_2}\|_1$$

Similarly, we have

$$\|\mathbf{v}_{\mathcal{D}_1} - \mathbf{v}_{\mathcal{D}_2}\|_{\infty} \leq \|\mathbf{v}_{\mathcal{D}_1} - \mathbf{v}_{\mathcal{D}_2}\|_1$$

Theorem 1 then follows.

Remark We need to clarify that the stability of persistence vector is not specific to the scalar function ρ defined in Eq (3). Our choice of ρ is a possible representative function that is easy to compute meanwhile has the following two conditions. First, the scalar function ρ satisfies the condition (5) in Lemma 1 can produce the stability theorem for persistence vectors. Second, the weight in ρ should be zero for the point in the diagonal of persistence diagram, which implies that this point is the topological noise and should be neglected in practical.

4. Representation with vanishing polynomials

Stability is not enough for machine learning. The persistence vectors in Eq. (4) with stability property can be considered as the feature representation of PDs. More importantly, the separability of such feature representation should be theoretically guaranteed when plugged into machine learning methods.

To obtain the linear separable features from persistence vectors, Gaussian or polynomial kernel is the standard way to map the vector space to the lifted space. However, the polynomial mapping of kernel needs to be pre-defined and therefore is suboptimal to any specific learning tasks. Moreover, the selection of appropriate kernel for task-oriented feature representation is tricky so as to achieve the satisfactory classification performance. To alleviate these problems, this section aims to learn the task-adapted and linearly separable feature representation, which captures the discriminative structure of the persistence vector. We also experimentally confirm the discriminative power of the proposed method and show that it outperforms conventional kernel methods.

4.1. Problem statement

In the following, we denote a *persistence vector set* as \mathbf{V} , in which each $\mathbf{v} \in \mathbf{V}$ is a persistence vector that is derived from a persistence diagram as in Eq. (4). Inspired by the vanishing ideal in [17, 23, 30], our approach builds upon the following assumption: *persistence vectors in \mathbf{V} are regarded as the roots of a polynomial system.* This assumption is useful to derive the *vanishing polynomial set*, which allows us to obtain the linearly separable feature underlying the persistence vectors.

Definition 3 The vanishing polynomial set $\mathcal{I}(\mathbf{V})$ is defined as a set of polynomials vanishing on persistence vectors \mathbf{V} .

$$\mathcal{I}(\mathbf{V}) = \{f \in \mathbb{R}[\mathbf{v}] : f(\mathbf{v}) = 0 \text{ for all } \mathbf{v} \in \mathbf{V}\} \quad (6)$$

where $\mathbb{R}[\mathbf{v}]$ denotes the space of all polynomials with real coefficients in vector \mathbf{v} .

Remark. With the definition of *vanishing polynomial set*, we can extract the linearly separable feature from PDs through the following two important procedures: The first step is to construct the vanishing polynomial set for the persistence vectors using Algorithm 1. The vanishing polynomial set can characterize the discriminative algebraic structure underlying the persistence vectors. By using the vanishing polynomial set, the second step is to derive the *polynomial representation* from for persistence vectors. We can prove that the resulting polynomial representation is linearly separable. This section also shows how the polynomial representation can be used for classification.

4.2. Vanishing polynomials of persistence vectors

We first give a step by step formulation for vanishing polynomials. Any degree- d polynomial can be decomposed into a sum of homogeneous polynomials as

$$f = \sum_{1 \leq i \leq d} \mathbf{w}_i \phi_i^T = (\mathbf{w}_1, \dots, \mathbf{w}_d) (\phi_1, \dots, \phi_d)^T = \mathbf{w} \Phi \quad (7)$$

where ϕ_d is a vector of degree- d homogeneous monomials, and \mathbf{w}_d is its coefficient vector. For example, given a 2-dimensional persistence vector $\mathbf{v} = (x, y)$, $f_1(\mathbf{v}) = -x + 3y + 6x^2 - 2xy + 7y^2 = 0$ in Fig. 1 induces $\mathbf{w}_1 = (-1, 3)$, $\phi_1(\mathbf{v}) = (x, y)$, $\mathbf{w}_2 = (6, -2, 7)$ and $\phi_2(\mathbf{v}) = (x^2, xy, y^2)$. In fact, ϕ_d is a degree- d Veronese map [21]:

$$\phi_d : (x_1, \dots, x_k) \mapsto (\dots, x_1^{i_1} \dots x_k^{i_k}, \dots) \quad (8)$$

where $i_1 + \dots + i_k = d$ means that the degree- d Veronese map sends $[x_1, \dots, x_k]$ to all possible monomials of total degree d . For example, $\phi_2(\mathbf{v})$ is the degree-2 Veronese map of x and y .

Degree- d polynomial matrix. Recall that our goal is to find a set of vanishing polynomials for persistence vectors. Given a set of persistence vectors $\mathbf{V} = \{\mathbf{v}_1, \dots, \mathbf{v}_m\}$ and polynomials $\Phi = (\phi_1, \phi_2, \dots, \phi_d)^T$, we first construct the following polynomial matrix

$$\Phi(\mathbf{V}) = [\Phi(\mathbf{v}_1), \dots, \Phi(\mathbf{v}_m)] \\ = \begin{pmatrix} \phi_1^T(\mathbf{v}_1) & \phi_1^T(\mathbf{v}_2) & \dots & \phi_1^T(\mathbf{v}_m) \\ \phi_2^T(\mathbf{v}_1) & \phi_2^T(\mathbf{v}_2) & \dots & \phi_2^T(\mathbf{v}_m) \\ \dots & \dots & \dots & \dots \\ \phi_d^T(\mathbf{v}_1) & \phi_d^T(\mathbf{v}_2) & \dots & \phi_d^T(\mathbf{v}_m) \end{pmatrix} \quad (9)$$

Algorithm 1 Vanishing polynomial set

Input: persistence diagrams $\{\mathcal{D}_1, \dots, \mathcal{D}_m\}$ within the same class, n , d and ϵ

Initialize: a set of persistence vectors $\mathbf{V} = \{\mathbf{v}_1, \dots, \mathbf{v}_m\} \in \mathbb{R}^{m \times n}$ via Eq. (4)

1: Build the degree- d polynomial matrix $\Phi(\mathbf{V})$ via Eq. (9)

2: Find null space by performing SVD on $\Phi(\mathbf{V}) = \mathbf{U}\Sigma\mathbf{W}^T$ via Eq. (11)

3: Compute the vanishing polynomial set with tolerance ϵ , i.e.,

$$\mathcal{I}(\mathbf{V}) \leftarrow \{\Phi(\mathbf{V})\mathbf{W}_i, \sigma_i < \epsilon\}$$

Output: Vanishing polynomials $\mathcal{I}(\mathbf{V})$

where $\phi_d(\mathbf{v}_i)$ is computed by the degree- d Veronese map on $\mathbf{v}_i \in \mathbf{V}$ according to Eq. (8). We restrict $\phi_d(\mathbf{v}_i)$ to the lower-degree polynomials, otherwise the higher degree will overfit the data.

Null space of $\Phi(\mathbf{V})$. Eq. (7) implies that f vanishes on persistence vectors \mathbf{V} if and only if the coefficient vector lies in the null space of $\Phi(\mathbf{V})$ in Eq. (9). That means the following relationship

$$f(\mathbf{V}) = \mathbf{W}\Phi(\mathbf{V}) = 0 \iff \mathbf{W} \in \text{null}(\Phi(\mathbf{V})) \quad (10)$$

A straightforward way to compute the null space of matrix is through singular value decomposition (SVD)

$$\Phi(\mathbf{V}) = \mathbf{U}\Sigma\mathbf{W}^T \quad (11)$$

Multiply Eq. (11) by an orthogonal matrix \mathbf{W} and obtain

$$\Phi(\mathbf{V})\mathbf{W} = \mathbf{U}\Sigma \quad (12)$$

We focus on the i -th column of \mathbf{W} and \mathbf{U} , i.e., $\Phi(\mathbf{V})\mathbf{W}_i = \mathbf{U}_i\sigma_i$. Denote that \mathbf{w}_i and \mathbf{u}_i are the i -th singular vector of \mathbf{W} and \mathbf{U} respectively. Scalar σ_i is the i -th singular value in the diagonal matrix Σ .

Compute vanishing polynomials. If the i -th singular value $\sigma_i = 0$, its singular vector \mathbf{W}_i lies in the null space of $\Phi(\mathbf{V})$. We can regard \mathbf{W}_i as a coefficient vector of the linear combination of the polynomials in Φ . Accordingly, the vanishing polynomials for \mathbf{V} can be computed as

$$\mathcal{I}(\mathbf{V}) = \{\Phi(\mathbf{V})\mathbf{W}_i \mid \mathbf{W}_i \text{ is a singular vector w.r.t. } \sigma_i = 0\} \quad (13)$$

The size of $\mathcal{I}(\mathbf{V})$ is equivalent to the number of zero singular values σ_i in the diagonal matrix Σ , according to Eq. (13). Therefore, we have the following relation

$$|\mathcal{I}(\mathbf{V})| = \#\{\sigma_i = 0\} \leq \text{rank}(\Sigma) = \text{rank}(\Phi(\mathbf{V})) \\ \leq \min(d, m) \leq m \quad (14)$$

which implies that the number of vanishing polynomials on \mathbf{V} is less than the sample size m . The pseudo-code of computing $\mathcal{I}(\mathbf{V})$ is summarized in Algorithm 1.

Remark. Perturbations in the persistence vectors \mathbf{V} are unavoidable due to the noisy PDs. It is unreasonable to seek zero singular values of $\Phi(\mathbf{V})$. Instead, we choose the right singular vectors of $\Phi(\mathbf{V})$ corresponding to near-zero singular values σ_i with ϵ -tolerance.

4.3. Linearly separable feature

Given s different classes of topological data, we can compute their corresponding s sets of PDs using the software DIPHA [3]. With these prepared PDs, our method begins with computing s categories of the persistence vectors $\{\mathbf{V}_1, \dots, \mathbf{V}_s\}$ via the persistence vectorization (Definition 2). Accordingly, s vanishing polynomial sets $\{\mathcal{I}_1(\cdot), \dots, \mathcal{I}_s(\cdot)\}$ can be derived by Algorithm 1. We now demonstrate that one can represent a persistence vector \mathbf{v} with these vanishing polynomial sets.

Definition 4 *The polynomial representation is a s -dimensional Euclidean vector that can be obtained through the mapping*

$$\mathbf{v} \mapsto (\|\mathcal{I}_1(\mathbf{v})\|_2, \|\mathcal{I}_2(\mathbf{v})\|_2, \dots, \|\mathcal{I}_s(\mathbf{v})\|_2) \in \mathbb{R}^s \quad (15)$$

where \mathbf{v} is the persistence vector, $\|\mathcal{I}_k(\cdot)\|_2$ is a vector norm and $\mathcal{I}_k(\cdot) = \{f_1, f_2, \dots, f_{|\mathcal{I}_k|}\}$ (computed by Algorithm 1) denotes the vanishing polynomial set of the k -th class persistence vectors.

The polynomial representation is a Euclidean vector with one significant property: if the persistence vector \mathbf{v} belongs to the k -th class, then the k -th component $\|\mathcal{I}_k(\mathbf{v})\|_2$ of its polynomial representation is zero. In contrast, other components $\|\mathcal{I}_l(\mathbf{v})\|_2$ are non-zero, where $l \neq k$. From this property, we can prove that the polynomial representation is linearly separable among different classes of persistence vectors.

Theorem 2 *The polynomial representation defined as Eq. (15) is linearly separable in the feature space $(\|\mathcal{I}_1(\cdot)\|_2, \dots, \|\mathcal{I}_s(\cdot)\|_2)$.*

Proof Case 1 ($s = 2$): *We assume two classes of persistence vectors, denoted as \mathbf{V}_1 and \mathbf{V}_2 . Their vanishing polynomial sets are $\mathcal{I}_1(\cdot)$ and $\mathcal{I}_2(\cdot)$, respectively. The polynomial representation of $\mathbf{v} \in \mathbf{V}_1$ and $\boldsymbol{\kappa} \in \mathbf{V}_2$ are*

$$\begin{cases} \mathbf{v} \mapsto (\|\mathcal{I}_1(\mathbf{v})\|_2, \|\mathcal{I}_2(\mathbf{v})\|_2) \\ \boldsymbol{\kappa} \mapsto (\|\mathcal{I}_1(\boldsymbol{\kappa})\|_2, \|\mathcal{I}_2(\boldsymbol{\kappa})\|_2) \end{cases} \quad (16)$$

Since all $\mathbf{v} \in \mathbf{V}_1$ are defined as the common roots of $\mathcal{I}_1(\cdot)$ rather than $\mathcal{I}_2(\cdot)$. Similarly, all $\boldsymbol{\kappa} \in \mathbf{V}_2$ are defined as the

common roots of $\mathcal{I}_2(\cdot)$ rather than $\mathcal{I}_1(\cdot)$. We can induce that

$$\begin{cases} \|\mathcal{I}_1(\mathbf{v})\|_2 = 0 \quad \text{and} \quad \|\mathcal{I}_2(\mathbf{v})\|_2 > \delta_1 > 0 \\ \|\mathcal{I}_2(\boldsymbol{\kappa})\|_2 = 0 \quad \text{and} \quad \|\mathcal{I}_1(\boldsymbol{\kappa})\|_2 > \delta_2 > 0 \end{cases} \quad (17)$$

Based on Eq. (17), we use two weight parameters $\lambda_1 > 0$ and $\lambda_2 < 0$ to obtain two inequalities.

$$\begin{cases} \lambda_1 \|\mathcal{I}_1(\mathbf{v})\|_2 + \lambda_2 \|\mathcal{I}_2(\mathbf{v})\|_2 < \lambda_2 \delta_1 < 0 \\ \lambda_1 \|\mathcal{I}_1(\boldsymbol{\kappa})\|_2 + \lambda_2 \|\mathcal{I}_2(\boldsymbol{\kappa})\|_2 > \lambda_1 \delta_2 > 0 \end{cases} \quad (18)$$

Eq. (18) indicates that the polynomial representations of \mathbf{v} and $\boldsymbol{\kappa}$ can be linearly separated by the classifier (λ_1, λ_2) .

Case 2 ($s > 2$): *Without loss of generality, we use the one-vs-the-rest strategy to prove the multiclass classification case. We randomly choose one class of persistence vectors as the first class and consider the rest as the second class. The multi-class problem is transformed into a two-class problem, which can be proved as in Case 1.*

5. Numerical results

Our work (or other TDA works) is actually complementary to traditional features rather than competing with them, and that is why we do not compare it with well-known feature representations (e.g., CNN). We follow the general practise in TDA research [7, 8, 26] and carry out a series of experiments comparing with popular TDA methods on tasks including texture recognition and protein analysis.

We compare our method with several popular TDA methods on classical benchmark datasets. For the input topological data, we construct their PDs of different classes using the software DIPHA [3], evaluate the discriminative capability of state-of-the-art TDA methods, and reveal the most effective vectorization of PDs when combined with machine learning techniques, e.g., LIBSVM [9] in our experiments. Parameter setting of all comparison methods will be first described.

PSS. Persistence scale space kernel [35] utilizes a multi-scale kernel function and maps PD into a Hilbert space that is appropriate for machine learning algorithms. This kernel function is defined by the solutions of heat diffusion equation at the points of PD. We choose the kernel scale parameter σ from $\{10^{-3}, 10^{-2}, 0.2, 1, 10, 50, 10^2, 10^3\}$.

PSR. Persistence square-root representation [2] models a PD as a probability density function (pdf) on the Hilbert Sphere. It then discretizes the pdf into a $K \times K$ grid. A smaller value of K reduces the accuracy, and a larger K improves the accuracy as well as the computational cost. Parameter K is chosen from the set $\{5, 10, 20, 50, 75, 100\}$.

PI. Persistence image [1] represents a PD as a finite-dimensional vector that is derived by the weighted kernel density estimation. The resolution parameter of the persistence image is selected from

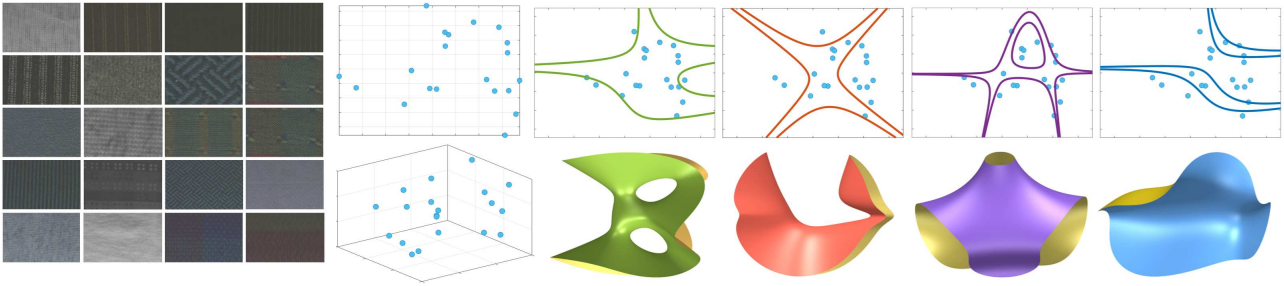


Figure 3. Persistence vectors and vanishing polynomials of textures labeled as “canvas”. When the dimension n of persistence vector is 2, the vanishing polynomials are algebraic curves. When the dimension $n = 3$, the vanishing polynomials are algebraic surfaces.

$\{5, 10, 20, 50, 75, 100\}$ and the kernel parameter is selected from $\{0.01, 0.05, 0.1, 0.15, 0.2\}$, resulting in $6 \times 5 = 30$ pairs of parameter settings.

PV. This method refers to the proposed persistence vectors in Eq. (4), which can be directly used for training vector-based classifier. The dimension of persistence vector is assigned from $n = 2$ to $n = 5$. Parameter C in Eq. (2) is 0.1 and σ in Eq. (3) is chosen from values $\{0.01, 0.5, 2, 10\}$.

PV+KER. This method uses a standard polynomial kernel to classify the proposed persistence vectors for comparison. The degree- t polynomial kernel is defined as $K(x, y) = (x^T y + 1)^t$ and t is chosen in range 2 to 5.

PV+POR. This is the proposed framework for PDs involves the persistence vectorization of Eq. (4) and the polynomial representation of Eq. (15). The degree d of polynomial in Eq. (9) is chosen in range 2 to 5.

5.1. Texture recognition

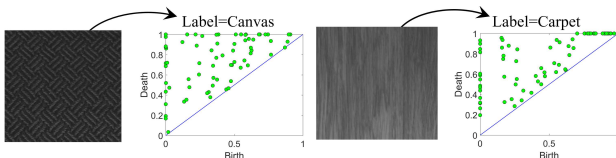


Figure 5. Two PDs from different texture classes.

Methods	Clbp-s	Clbp-m
PSS	70.5 ± 2.9	56.2 ± 2.3
PSR	68.4 ± 1.6	54.3 ± 0.9
PI	72.1 ± 1.3	57.8 ± 1.6
PV	71.8 ± 1.5	55.8 ± 1.1
PV+KER	72.2 ± 1.2	57.3 ± 1.2
PV+POR	75.3 ± 1.0	62.3 ± 1.4

Table 1. Texture recognition results (%).

We carry out the texture recognition tasks on the benchmark dataset OUTEX00000 [32], which includes 480 texture images equally classified into 24 classes and provides 100 predefined training/testing splits. Following the setting in [35], texture images are downsampled to 32×32 images. We apply CLBP [19] to describe each local region on an image as two discretized components named as Sign (CLBP-S) and Magnitude (CLBP-M). We construct PDs for

the component CLBP-S or CLBP-M. Fig. 5 gives two examples of PDs for texture images labeled as “canvas” and “carpet”. The “canvas” class of 20 textures corresponds to 20 persistence vectors of different dimension, i.e., 20 blue points in the 2-dimensional and 3-dimensional space. Accordingly, Fig. 3 shows that the vanishing polynomials of the persistence vectors are algebraic curves ($n = 2$) and algebraic surfaces ($n = 3$). For the visualization purpose, not all of the vanishing polynomials are shown in the Fig. 3.

Texture recognition results are reported in Table 1. All methods achieve significantly better results on the component CLBP-S because CLBP-S is more informative than CLBP-M. It is observed that our method (PV+POR) outperforms all comparison methods. Although CLBP is sensitive to noise [19] and this will result in the perturbations in PDs, PV+POR can remedy such perturbations via the stable persistence vectorization. Furthermore, PV+POR can extract the polynomial representation from this stable vectorization that will greatly benefits the further analysis. We see that PV+KER achieves higher recognition rates than PV but less than PV+POR. This verifies that polynomial kernel can make the persistence vector easier to classify in the lifted space. However, results of PV+KER are suboptimal to PV+POR. This is mainly because PV+KER depends on the kernel with the pre-defined polynomial, which may be inappropriate for texture recognition. In contrast, our polynomial presentation (PV+POR) can extract the preferable and flexible polynomials from persistence vectors, which can benefit recognition tasks. Lastly, the worst performance of PSR further confirms that the Hilbert sphere manifold is not robust to the perturbations caused by CLBP. Experimental comparisons with these baselines shows that constructing task adapted polynomials representation is indeed necessary for achieving satisfying recognition performance.

5.2. Protein analysis

The second experiment is to analyze the geometric shape of the protein called hemoglobin, which is important for analyzing the oxygen transport and bind [6]. The benchmark dataset contains 3D hemoglobin shapes from Protein

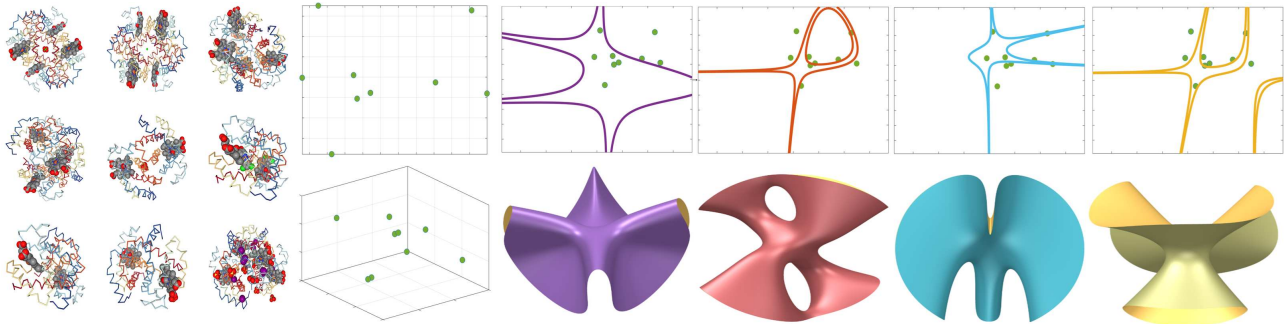


Figure 4. Persistence vectors and vanishing polynomials of proteins labeled as “Relaxed”. When the dimension n of persistence vector is 2, the vanish polynomials are algebraic curves. When the dimension $n = 3$, the vanish polynomials are algebraic surfaces.

Data Bank (PDB) ¹. These hemoglobin shapes exist in one of two conformations known as the Relaxed form and the Taut form. In total, we use 9 Relaxed forms and 10 Taut forms of hemoglobin. We select one hemoglobin data from each form as testing data, and use the remaining as training data. Consequently, 90 runs are performed and the accuracy is calculated via the cross-validation. Fig. 6 gives two examples of PDs for hemoglobin proteins labelling Taut form and Relaxed form. Fig. 4 shows some examples of vanishing polynomials for Relaxed class. When the dimension n of persistence vector is 2, the vanishing polynomials are algebraic curves. When the dimension $n = 3$, the vanishing polynomials are algebraic surfaces.

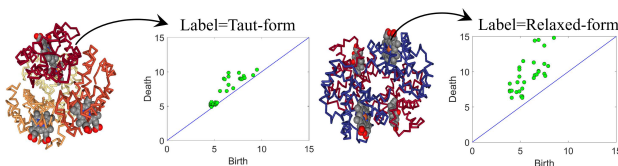


Figure 6. Two PDs from different protein classes.

Methods	Relaxed	Taut
PSS	83.2 ± 1.6	92.3 ± 1.4
PSR	82.4 ± 0.8	93.7 ± 1.2
PI	85.1 ± 1.2	92.7 ± 0.9
PV	82.9 ± 1.4	92.1 ± 1.6
PV+KER	84.2 ± 1.3	92.6 ± 1.4
PV+POR	86.7 ± 0.9	94.7 ± 0.8

Table 2. Protein recognition results (%).

The averaged classification accuracy of 90 independent runs is reported in Table 2. Our method (PV+POR) achieves the highest average accuracy in both protein forms, with the accuracy of 86.7% for the Relaxed form and 94.7% for the Taut form. Note that the expensive cost of protein collection leads to those small-scale benchmark datasets for protein analysis. As we know, the small-scale data are not preferred when training the classifier. Our method alleviates this issue by extracting linear separable feature that is easy to be distinguished among different classes of proteins. In con-

trast, the compared TDA methods conventionally assume that the long-persistent topological components are significant for classification, while the short-persistent topological components should be discarded as noise. However, both the global and the local features are equally important to characterize different proteins structures [37, 39].

6. Conclusion

Persistent diagram (PD) is a topological data analysis tool which performs multi-scale analysis on topological structures. This paper proposes a novel algebraic representation for PDs and complements standard feature representations for machine learning, which is proved to be stable and linearly separable. Specifically, an efficient and stable persistence vectorization is proposed to transform PDs into the Euclidean vectors called the persistence vectors. Persistence vector preserves the significance of each topological feature encoded in PDs, which is proved to be stable with the perturbations of PDs. Compared with existing TDA methods which only provide the pre-defined feature map, our method goes beyond and exploits the flexible polynomial representation from the persistence vector. In addition, a simple approximation algorithm is proposed to compute the polynomial representation. Most significantly, we can prove that the proposed polynomial representation is linearly separable. We also confirm experimentally the discriminative capability of the polynomial representation in several classification problems.

At present, our method adopts the singular vector decomposition (SVD) to construct vanishing polynomials. This may increase the computational complexity of vanishing polynomials with the larger degree. In fact, other strategies such as randomized SVD [20] or partial SVD [27] might be possible and better suited for efficiency purpose.

Acknowledgment: This work was supported by the International Cooperation Project of Institute of Information Engineering, Chinese Academy of Sciences under Grant No.Y7Z0511101 and Australian Research Council Linkage Project (LP170100891, LP140100937).

¹<https://www.rcsb.org>

References

- [1] H. Adams, T. Emerson, M. Kirby, R. Neville, C. Peterson, P. Shipman, S. Chepushtanova, E. Hanson, F. Motta, and L. Ziegelmeier. Persistence images: a stable vector representation of persistent homology. *Journal of Machine Learning Research*, 18(8):1–35, 2017.
- [2] R. Anirudh, V. Venkataraman, K. Natesan Ramamurthy, and P. Turaga. A riemannian framework for statistical analysis of topological persistence diagrams. In *Proceedings of the IEEE Conference on Computer Vision and Pattern Recognition Workshops*, pages 68–76, 2016.
- [3] U. Bauer, M. Kerber, and J. Reininghaus. Distributed computation of persistent homology. In *2014 Proceedings of the Sixteenth Workshop on Algorithm Engineering and Experiments (ALENEX)*, pages 31–38. SIAM, 2014.
- [4] L. Bigo, M. Andreatta, J.-L. Giavitto, O. Michel, and A. Spicher. Computation and visualization of musical structures in chord-based simplicial complexes. In *International Conference on Mathematics and Computation in Music*, pages 38–51. Springer, 2013.
- [5] T. Bonis, M. Ovsjanikov, S. Oudot, and F. Chazal. Persistence-based pooling for shape pose recognition. In *International Workshop on Computational Topology in Image Context*, pages 19–29. Springer, 2016.
- [6] Z. Cang, L. Mu, K. Wu, K. Opron, K. Xia, and G.-W. Wei. A topological approach for protein classification. *Molecular Based Mathematical Biology*, 3(1), 2015.
- [7] M. Carriere, M. Cuturi, and S. Oudot. Sliced wasserstein kernel for persistence diagrams. In *Proceedings of the 34th International Conference on Machine Learning-Volume 70*, pages 664–673. JMLR.org, 2017.
- [8] M. Carrière, S. Y. Oudot, and M. Ovsjanikov. Stable topological signatures for points on 3d shapes. In *Computer Graphics Forum*, volume 34, pages 1–12. Wiley Online Library, 2015.
- [9] C.-C. Chang and C.-J. Lin. Libsvm: a library for support vector machines. *ACM transactions on intelligent systems and technology (TIST)*, 2(3):27, 2011.
- [10] F. Chazal, B. Fasy, F. Lecci, B. Michel, A. Rinaldo, A. Rinaldo, and L. Wasserman. Robust topological inference: Distance to a measure and kernel distance. *The Journal of Machine Learning Research*, 18(1):5845–5884, 2017.
- [11] F. Chazal, B. T. Fasy, F. Lecci, A. Rinaldo, and L. Wasserman. Stochastic convergence of persistence landscapes and silhouettes. In *Proceedings of the thirtieth annual symposium on Computational geometry*, page 474. ACM, 2014.
- [12] F. Chazal, M. Glisse, C. Labrière, and B. Michel. Convergence rates for persistence diagram estimation in topological data analysis. *The Journal of Machine Learning Research*, 16(1):3603–3635, 2015.
- [13] D. Cohen-Steiner, H. Edelsbrunner, and J. Harer. Stability of persistence diagrams. *Discrete & Computational Geometry*, 37(1):103–120, 2007.
- [14] T. Dey, S. Mandal, and W. Varcho. Improved image classification using topological persistence. In *Proceedings of the conference on Vision, Modeling and Visualization*, pages 161–168. Eurographics Association, 2017.
- [15] B. Di Fabio and M. Ferri. Comparing persistence diagrams through complex vectors. In *International Conference on Image Analysis and Processing*, pages 294–305. Springer, 2015.
- [16] H. Edelsbrunner and J. Harer. *Computational topology: an introduction*. American Mathematical Soc., 2010.
- [17] J. B. Farr and S. Gao. Computing gröbner bases for vanishing ideals of finite sets of points. In *International Symposium on Applied Algebra, Algebraic Algorithms, and Error-Correcting Codes*, pages 118–127. Springer, 2006.
- [18] M. Ferri. Persistent topology for natural data analysis a survey. In *Towards Integrative Machine Learning and Knowledge Extraction*, pages 117–133. Springer, 2017.
- [19] Z. Guo, L. Zhang, and D. Zhang. A completed modeling of local binary pattern operator for texture classification. *IEEE Transactions on Image Processing*, 19(6):1657–1663, 2010.
- [20] N. Halko, P.-G. Martinsson, and J. A. Tropp. Finding structure with randomness: Probabilistic algorithms for constructing approximate matrix decompositions. *SIAM review*, 53(2):217–288, 2011.
- [21] J. Harris. *Algebraic geometry: a first course*, volume 133. Springer Science & Business Media, 2013.
- [22] A. Hatcher. *Algebraic topology*. Citeseer, 2001.
- [23] D. Heldt, M. Kreuzer, S. Pokutta, and H. Poulisse. Approximate computation of zero-dimensional polynomial ideals. *Journal of Symbolic Computation*, 44(11):1566–1591, 2009.
- [24] C. Hofer, R. Kwitt, M. Niethammer, and A. Uhl. Deep learning with topological signatures. In *Advances in Neural Information Processing Systems*, pages 1633–1643, 2017.
- [25] K. Hu and L. Yin. Multi-scale topological features for hand posture representation and analysis. In *Proceedings of the IEEE International Conference on Computer Vision*, pages 1928–1935, 2013.
- [26] G. Kusano, Y. Hiraoka, and K. Fukumizu. Persistence weighted gaussian kernel for topological data analysis. In *International Conference on Machine Learning*, pages 2004–2013, 2016.
- [27] R. M. Larsen. Lanczos bidiagonalization with partial re-orthogonalization. *DAIMI Report Series*, 27(537), 1998.
- [28] C. Li, M. Ovsjanikov, and F. Chazal. Persistence-based structural recognition. In *Proceedings of the IEEE Conference on Computer Vision and Pattern Recognition*, pages 1995–2002, 2014.
- [29] J.-Y. Liu, S.-K. Jeng, and Y.-H. Yang. Applying topological persistence in convolutional neural network for music audio signals. *arXiv preprint arXiv:1608.07373*, 2016.
- [30] R. Livni, D. Lehavi, S. Schein, H. Nachliely, S. Shalev-Shwartz, and A. Globerson. Vanishing component analysis. In *International Conference on Machine Learning*, pages 597–605, 2013.
- [31] J. L. Nielson, J. Paquette, A. W. Liu, C. F. Guandique, C. A. Tovar, T. Inoue, K.-A. Irvine, J. C. Gensel, J. Kloke, T. C. Petrossian, et al. Topological data analysis for discovery in preclinical spinal cord injury and traumatic brain injury. *Nature communications*, 6:8581, 2015.
- [32] T. Ojala, T. Menp, M. Pietikinen, J. Viertola, J. Kyllnen, and S. Huovinen. Outex - new framework for empirical evalua-

- tion of texture analysis algorithms. In *International Conference on Pattern Recognition, 2002. Proceedings*, pages 701–706 vol.1, 2002.
- [33] F. T. Pokorny, H. Kjellström, D. Kragic, and C. Ek. Persistent homology for learning densities with bounded support. In *Advances in Neural Information Processing Systems*, pages 1817–1825, 2012.
- [34] S. T. Rachev and L. Rüschendorf. *Mass Transportation Problems: Volume II: Probability and its Applications*. Springer Science & Business Media, 1998.
- [35] J. Reininghaus, S. Huber, U. Bauer, and R. Kwitt. A stable multi-scale kernel for topological machine learning. In *Proceedings of the IEEE conference on computer vision and pattern recognition*, pages 4741–4748, 2015.
- [36] L. Wasserman. Topological data analysis. *Annual Review of Statistics and Its Application*, 5:501–532, 2018.
- [37] L. Wei and Q. Zou. Recent progress in machine learning-based methods for protein fold recognition. *International journal of molecular sciences*, 17(12):2118, 2016.
- [38] K. Xia and G.-W. Wei. Persistent homology analysis of protein structure, flexibility, and folding. *International journal for numerical methods in biomedical engineering*, 30(8):814–844, 2014.
- [39] J.-Y. Yang and X. Chen. Improving taxonomy-based protein fold recognition by using global and local features. *Proteins: Structure, Function, and Bioinformatics*, 79(7):2053–2064, 2011.
- [40] X. Zhu. Persistent homology: An introduction and a new text representation for natural language processing. In *IJCAI*, pages 1953–1959, 2013.